Robust control based on linear matrix inequalities criterion of single phase distributed electrical energy systems operating in islanded and grid-connected modes

Allal El Moubarek Bouzid, Hicham Chaoui, Mohamed Zerrougui, Seifeddine Ben Elghali, Mohamed Benbouzid

Version of Record: https://www.sciencedirect.com/science/article/pii/S0306261921002804
Manuscript_bc500edaa5639a574611ab805c30bc28

Robust Control Based on LMI Criterion of Single Phase Distributed Electrical Energy Systems Operating in Islanded and Grid-Connected Modes

Allal El Moubarek BOUZID[1], Hicham CHAOUI[2], Mohamed ZERROUGUI[3], Seifeddine BEN ELGHALI[3], and Mohamed BENBOUZID[4,5]

[1] *École Centrale de Nantes-LS2N, UMR CNRS 6004, 44321 Nantes, France; Allal-El-Moubarek.Bouzid@ec-nantes.fr*
[2] *Intelligent Robotic and Energy Systems (IRES), Department of Electronics, Carleton University, Ottawa, ON K1S 5B6, Canada;*
[3] *Laboratory of Information and Systems (LIS-UMR CNRS 7020), Aix-Marseille University, Marseille, France;*
[4] *Institut de Recherche Dupuy de Lôme (UMR CNRS 6027 IRDL), University of Brest, 29238 Brest, France;*
[5] *Engineering Logistics College, Shanghai Maritime University, Shanghai 201306, China*

Abstract

In this paper, a control strategy of a voltage source inverter with LCL filter in Distributed Electrical Energy Systems in both operation modes is proposed for microgrids environment. This robust control strategy considers a state feedback controller based on proportional resonant controller using Linear Matrix Inequalities. The controller is able to ensure a good tracking of sinusoidal references and to suppress low order harmonics. It allows to ensure simultaneously a robust stability of the system in front of external disturbances (grid disturbances, load variations), parametric uncertainty (grid inductance) and smooth transition (with no hazardous transients) between grid connected and islanded mode operation. In order to demonstrate the efficiency and performance of the proposed control strategy, a real time simulation using OP5600 from OPAL-RT is used. Several cases study are verified in real time and the results are analyzed and discussed.

Keywords: PR compensators, Distributed generation, Microgrid, LCL filter, Grid connected.

1. Introduction

Distributed generation is a widely known subject at the industrial and academic level, with specific norms for its regulation, with fundamental aspects being the limitation of harmonic content and protection against islanding [1][2]. It is precisely within the current trend of distributed generation that the concept of microgrid is introduced based on a set of low power distributed loads and sources, also called micro-sources, controlled as a single system capable of continuously meeting local energy demands [3]. That is, a system that, like all distributed generation, is designed to operate with connection to the power grid, but that can also operate in its absence as an island of energy, which is known as the island mode of operation [4] [5]. However, current standards such as International Standard 62116 of the International Electrotechnical Commision - IEC (2014) do not include the isolated operation of a hypothetical micro grid. In the event of an absence of the power grid, whether programmed or due to a disturbance, all distributed generation must be disconnected, this procedure being known as anti-island protection. The possibility of operating in an isolated manner appears as an attractive alternative and with important advantages, such as the continuous meeting of the demand for local load and the possibility of assisting in the restoration of the system, after a blackout [6].

In the specific case of distributed sources of the direct current (DC) type, such as PV systems, fuel cell, battery banks and high frequency alternating current (AC) systems (microturbines), whose output is normally rectified, the generated

energy needs to be previously processed to be used by local loads and / or injected into the power grid [7]. To perform this processing, power electronics converters are used that adapt voltage and current to the corresponding alternating current requirements. The most used converter topology for this purpose is the Voltage Source Inverter - VSI [8]. The use of switched converters leads to the appearance of harmonic components that, in addition to being undesirable, are limited by standards such as the Standard for Interconnecting Distributed Resources with Electric Power Systems of the Institute of Electrical and Electronics Engineers - IEEE (2008), known as IEEE 1547, or the international standard 61727 of IEC (2004), known as IEC 61727. Therefore, it is necessary to use filters to reduce this content, the two most common topologies are the L filter and the LCL filter. The L filters have a first order behavior with simplicity in the control and attenuation of 20 dB / dec. However, with this type of filter it is not possible to adjust the output voltage. The LCL filters present an attenuation of 60 dB / dec, which translates into lower inductance values, resulting in less weight and volume of the system. In addition, this configuration makes it possible to adjust the output voltage in island mode, making it suitable for generation in the microgrid environment. However, the system presents a resonant behavior, which increases the complexity of the control with interactions between distributed electrical energy systems that can result in multiple resonances [9]. The increasing of these multiple resonances is also related by the connection of nonlinear and unbalanced electronic load appliances to the microgrid [10], which can affects negatively the power quality by increasing losses which can even lead to microgrid instability [11] [12].

Therefore, to guarantee the stability of the system, it is necessary to attenuate the high gain around the resonance frequency. For this purpose, damping techniques, classified as passive and active, are used. The former consider the inclusion of an additional element that dissipates the energy associated with the resonance. Logically, this implies additional losses. Active damping techniques, on the other hand, use control procedures, variable feedback, to suppress the high gain in the closed loop system. In addition to ensuring stability, the control system of an inverter for distributed generation applications performs the following tasks: carrying out the DC-AC conversion providing sinusoidal current with minimum frequency deviation and reduced harmonic content, protection of the distributed generation source and electrical grid in the face of any irregularity, and management of distributed generation (tracking the maximum power point, following the power reference to be injected) [13] [14].

In the literature, several researches contributing to damping and resonance analysis have been proposed [15]. A classical multi-loop control techniques based on conventional Proportional Integral (PI) controller have been proposed in [16] [17]. However, the PI control work for one operating point and in large scale system several operating points can be present, in this case the performances are not guaranteed and stability margin is reduced. A Proportional Resonant controller (PR) have been proposed in [18] to avoid the steady-state and phase shift problems. In order to obtain a wider damping region, the authors in [19], have proposed feedback based method by using complementary control loops by injecting either the capacitor current or voltage through a high pass filter [20]. Similary to the above method, in [21], the authors have proposed to use the filter inductor current to achieve the desired damping performances. However, these methods need more measurements with an increasing complexity of the control, which can limits the practical implementation and increase its cost [22]. In [23], [24], and [25], the root-loci-based approach have been proposed for

designing the controller to depict system stability. This approach take into account a single control parameter varying and the others system parameters are fixed. However, this method has a major drawback because in real system several control parameters vary and influence system stability simultaneously. The nonlinear control techniques have been proposed by several researches. The feedback linearization control method in [26]. However, this method use feedback variables derivatives that reduce control performances in transient modes. The Sliding Mode Control (SMC) was proposed in [27]. This method is robust and improve resonant phenomena, but the chattering effect and alter the system reliability. The intelligent controllers have been proposed in [28] for interactive learning control, in [29] for the neural grid control and in [30] for the repetitive control. However, these methods require complex algorithms with slow response time due their learning algorithm. In [31] a nonlinear backstepping design method based on the principle of preserving the high-order nonlinearity of the system was proposed to keep system stable and reduce the influence of the harmonic resonance over a wide range variation of control parameter.A finite-set model predictive control (FSMPC) with adaptive cost function was proposed in [32] for resonance suppression but Requires a precise model of the filter to reach the desired performance and needs a lot of calculations. To improve stability region, a dual current feedback active damping scheme in which both inverter current feedback and grid current feedback are proposed in [33], but designing appropriate gains for both feedback schemes is a challenging task. A robust grid current resonance suppression method was proposed in [34], it use a full duty ratio and zero-beat-lag pulse width modulation scheme to mitigate the control and computational delays. In [35], an adaptive method to tune a virtual resistor was proposed to eliminate the issue of resonance and stabilize the system. In [36], the capacitor feedforward voltage was used to suppress the resonance but creates a new resonance if the appropriate computational delay is not added in the feedback loop of the controller. In [37], estimate the capacitor current was performed directly from the model depending on the derivative of the measured current, where inverter side current is used as feedback; however, differentiation of measured current will amplify the noise. The full state observer is used in [38] with measuring grid side current and an additional lead lag network to compensate control delay. The notch filter to eliminate resonance harmonics components in inverter output voltage is used in [39]. However, the notch filter must be tuned carefully since erroneous tuning will compromise the LCL-filter stability. It remain sensitive to parameters uncertainties and its efficiency depends on the accuracy of the resonance frequency estimate. In [40], a current decoupling control scheme based on extended state observer module, nonlinear controller and tracking differentiator module was proposed to achieve a good performance and improves an active damping, but this method become more complex by adding decoupling control scheme . A fast deadbeat algorithm with a fixed switching frequency was propoded in [41]. It allow to predict and control the grid-connected current, this algorithm can effectively compensate the system delay, but there is still a limitation of relying on accurate electrical parameters.

However, in the specific case of an inverter to be used for distributed generation in the microgrid environment, the possibility of operating in the islanded system must be added as a task to the control system, providing a sinusoidal voltage with low harmonic content and amplitude and frequency fixed. In addition, the system must carry out smooth transitions between operating modes, when switching from island operation to that connected to the grid, and vice versa, guaranteeing the energy demanded by local loads without exposing them to transients that may damage them [6]. All of these tasks must

be met even under external disturbances such as changes in local load (in island mode), harmonic distortion and minor disturbances in the grid voltage (in the grid-connected mode) or fluctuations in the voltage supplied by the generating source (in both operating modes). However, it should be noted that, in systems connected to the electrical grid, the dynamics of the LCL filter is influenced by the grid inductance, whose value is uncertain [42]. All of these considerations must be taken into account when designing the control system [13]. There are several control strategies in the literature for inverters with LCL filters to be used in distributed generation, however, these cases are limited to the operation connected to the grid. In addition, the control of VSI systems with resonant output filters (LC or LCL) for autonomous operation is also a known issue. However, the control of systems capable of operating in both modes is a topic to be studied.

In this context, this paper a proposes two main contributions: a robust control voltage/current strategy for single-phase inverter, with LCL output filter to improve an active damping and avoid resonant phenomena. A two control loops voltage and current work in parallel to improve performances in grid connected and islanded mode environements with smooth transition among them for distributed generation. The proposed robust control strategy is based on state feedback by performing the resonance damping by active means considering two loops (voltage/current) operating in parallel in order to ensure the operation of the system in autonomous mode and in the mode connected to the grid. This strategy proposes the synthesis of feedback gains by means of Linear Matrix Inequalities (LMIs), considering simultaneously the criteria of robust stability, pole allocation and disturbance rejection to guarantee the stability of the system and certain performance criteria, such as the need to track sinusoidal references (current and voltage), the rejection of disturbances with zero error and the active and reactive powers control in the grid connected mode, as well as in island mode operation with low THD. The remainder of this paper is structured as follows. Section II gives the system description and modeling. Section III presents a proportional resonant control. Section IV outlines control based on active damping method. Section V presents the proposed robust control based on LMI criterion followed by robust control scheme of Distributed Electrical Energy Systems (DEES) in section VI.The effectiveness of the proposed controller is demonstrated through various real time simulations in Section VII. Finally, this paper concludes in Section VIII.

2. System Description and Modeling

The schematic shown in figure 1 is considered where the main variables to be considered in the analysis are: currents i_1 and i_2, voltages v_C and v_g, and the modulating signal $PWM(d)$.

2.1. Standalone operation

In this mode of operation the variable to be controlled is the voltage on the capacitor. Thus, it is possible to consider the output inductor L_2 as part of the load, reducing the equivalent circuit of the system to a VSI with LC output filter controlled as a voltage source [43], where the dynamics of the load is represented from the current i_2. Therefore, taking into account the average model of the VSI in a switching period, the system can be represented by the equivalent circuit of figure 1. In this circuit, the series resistance of the inductive elements is included. The equivalent circuit allows to

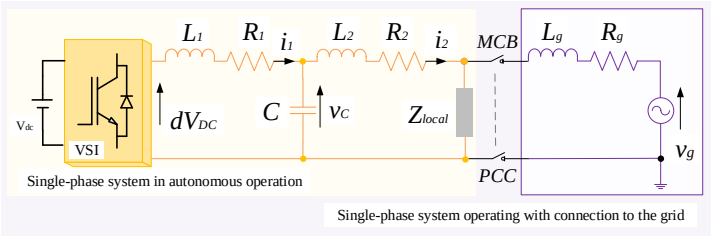

Figure 1: Equivalent circuit of the single-phase DER system for both operation modes

represent the dynamics according to (1) and (2).

$$L_1 \frac{di_1}{dt} = -R_1 i_1 - v_C + dV_{DC} \tag{1}$$

$$C \frac{dv_C}{dt} = i_1 - i_2 \tag{2}$$

As mentioned, the control input of the system is the cyclic ratio (d), however the controlled output is the voltage v_C. It is important to note that according to (2) the current i_2 would not be a state variable, but a disturbance. On the other hand, in (1) the effect of disturbances in the DC bus voltage can be included by adding the nonlinear term corresponding to the product of the alternating component in the DC bus and the cyclic ratio. However, this term can be considered as a disturbance (Δv_{DC}), reaching the expression (3).

$$L_1 \frac{di_1}{dt} = -R_1 i_1 - v_C + dV_{DC} + \Delta v_{DC} \tag{3}$$

Therefore, the dynamics described by (2) and (3) can be represented in state space using (4) or in a block diagram as shown in figure 2 [43] [44]. This diagram includes the current of the i_C capacitor. In both cases, the output variable (to be controlled) is considered to be the capacitor voltage.

$$\begin{aligned} \dot{\mathrm{x}}_v &= A_v \mathrm{x}_v + B_v \mathrm{u}_v + H_v \mathrm{w}_v \\ \mathrm{y}_v &= C_v \mathrm{x}_v \end{aligned} \tag{4}$$

$$\text{Where : } \mathrm{x}_v = \begin{bmatrix} i_1 \\ v_C \end{bmatrix},\ \mathrm{u}_v = d,\ C_v = [0\ 1],\ \mathrm{w}_v = \begin{bmatrix} i_2 \\ \Delta v_{DC} \end{bmatrix}$$

$$A_v = \begin{bmatrix} -\frac{R_1}{L_1} & -\frac{1}{L_1} \\ \frac{1}{C} & 0 \end{bmatrix},\ H_v = \begin{bmatrix} 0 & \frac{1}{L_1} \\ -\frac{1}{C} & 0 \end{bmatrix},\ B_v = \begin{bmatrix} \frac{V_{DC}}{L_1} \\ 0 \end{bmatrix},$$

2.2. Grid-connected operation

Considering the diagram of figure 2 with the miniature circuit breaker (MCB) device closed and the average model in a switching period for the VSI, the system can be represented by the equivalent circuit of figure 1. To the variables considered in the autonomous operation, the voltage of the grid v_g is added. Without loss of generality, in the present analysis, the effect of grid resistance R_g is disregarded. Therefore, based on the equivalent circuit of figure 1, it is possible

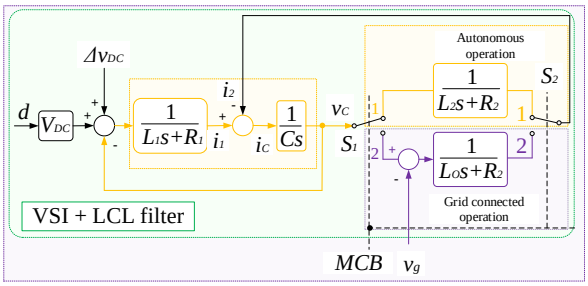

Figure 2: Block diagram for single-phase system for both operation modes

to represent the behavior of the system using equations (5) to (8). It is observed that the local load has no influence on the dynamics of the output current, and that this depends only on the voltage drop in the impedance of connection to the grid.

$$L_1 \frac{di_1}{dt} = -R_1 i_1 - v_C + dV_{DC} + \Delta v_{DC} \tag{5}$$

$$C \frac{dv_C}{dt} = i_1 - i_2 \tag{6}$$

$$L_O \frac{di_2}{dt} = v_C - R_2 i_2 - v_g \tag{7}$$

$$L_O = L_2 + L_g \tag{8}$$

It is important to note that this set of equations includes the expressions (2) and (3) corresponding to the autonomous operation of the system. This relationship is also manifested in the state-space representation (9) as well as in the block diagram of figure 2 [43] [44] [12]. In this case, the current variable i_2 is considered as the output variable.

$$\begin{aligned} \dot{\mathrm{x}}_c &= A_c \mathrm{x}_c + B_c \mathrm{u}_c + H_c \mathrm{w}_c \\ \mathrm{y}_c &= C_c \mathrm{x}_c \end{aligned} \tag{9}$$

$$\text{Where : } \mathrm{x}_c = \begin{bmatrix} i_1 \\ v_C \\ i_2 \end{bmatrix}, \mathrm{u}_c = d, \mathrm{w}_c = \begin{bmatrix} \Delta v_{DC} \\ v_g \end{bmatrix}, C_v = [0\ 0\ 1]$$

$$A_c = \begin{bmatrix} -\frac{R_1}{L_1} & -\frac{1}{L_1} & 0 \\ \frac{1}{C} & 0 & -\frac{1}{C} \\ 0 & \frac{1}{L_O} & -\frac{R_O}{L_O} \end{bmatrix}, \ B_c = \begin{bmatrix} \frac{V_{DC}}{L_1} \\ 0 \\ 0 \end{bmatrix}, H_c = \begin{bmatrix} \frac{1}{L_1} & 0 \\ 0 & 0 \\ 0 & -\frac{1}{L_0} \end{bmatrix}$$

3. Proportional Resonant control

Traditionally, tracking systems use components that integrate the error signal in order to cancel it permanently. This method is effective when the reference signals are constant over time. In the case of periodic references, such as those used in distributed generation systems, the tracking error is not null and increases as the frequency of the reference signal approaches the crossing frequency of the controlled system [43] [45]. In the case of disturbance rejection,

controllers based on integrators (PI, PID and others) guarantee a high rejection as long as the disturbances have reduced dynamics (low frequency), and can even amplify the disturbances of higher frequencies. These limitations are important in distributed generation systems where delays in tracking are undesirable and possible disturbances in the mains voltage would lead to the appearance of harmonics in the generated current [46] [47]. As an alternative, more resonant proportional control is introduced [48] [49]. This method aims to obtain a controller in the stationary coordinate system that presents the characteristics of a PI type controller designed in the synchronous coordinate system, that is, an integrator tuned to a certain frequency called resonance [43] [46] [49]. This idea derives from the internal sinusoidal model criterion presented in [50]. Considering a control system with a sinusoidal reference signal, based on the principle of the internal model, a compensator with a sinusoidal transfer function is required to guarantee tracking [50]. Therefore, in the Laplace domain, there are two options corresponding to the cosine (10) and sine (11) transforms.

$$G_1(s) = \frac{s}{s^2 + \omega_0^2} \tag{10}$$

$$G_2(s) = \frac{\omega_0}{s^2 + \omega_0^2} \tag{11}$$

Although the two expressions guarantee the tracking of sinusoidal signals with frequency ω_0, the expression (10) presents a faster dynamics due to the presence of a zero at the origin [46] [49]. Expressions (10) and (11) show infinite gain in the resonance frequency, which, tuned in the frequency of the reference signals, guarantees the tracking with null error. However, very high gains can be difficult to implement considering digital platforms. An alternative expression is presented in (12) where the damping coefficient ζ has been introduced, with which the designer can limit the gain in the resonance frequency [51] [46].

$$G_R(s) = \frac{s}{s^2 + 2\zeta\omega_0 s + \omega_0^2} \tag{12}$$

The resonant components are commonly used in the design of controllers called proportional plus resonant (PR) where a term of type (12) is used to replace the integral term of traditional PI controllers. In this case, the resonance frequency ω_0 is established to track the references [46] [12]. According to (12), a resonance frequency of 60 Hz and a damping coefficient of $10e^{-4}$ were considered. Controllers based on the expression (12) show considerable rejection of disturbances in the resonance frequency. This fact can be used to introduce additional components in the frequencies that are expected to appear disturbances, or where it is critical to reject them. Such is the case for DEES systems where it is normally required to meet limits on the harmonic components of the generated current [52] [53]. Thus, in the controller to be projected, in addition to the proportional and resonant components at the reference frequency, resonant components can be added at the frequencies of the main harmonics [43] [44]. Therefore, a PR controller with components for harmonic suppression features a transfer function such as that presented in (13) [43] [52], where index n indicates the order of the harmonic component considered , with K_p and K_{Rn} being the proportional and resonant gains of the harmonic component n. Alternatively, it is possible to represent the dynamics of the resonant controller in the state space according to (15). Where $\mathbf{x}_n$ is the state vector of the resonant controller in the harmonic component n, and the variable e is the tracking

error. The tracking error transfer functions for the controller states reproduce the expressions (10) and (11) respectively.

$$G_{PR}(s) = K_p + \sum_{n=1}^{h} \frac{K_{Rn} s}{s^2 + 2\zeta\omega_n s + \omega_n^2} \qquad (13)$$
$$\omega_n = n\omega_0$$

$$\begin{cases} \dot{\mathbf{x}}_{CR_n} = \boldsymbol{A}_{CR_n}\mathbf{x}_{CR_n} + \boldsymbol{B}_{CR_n} e \\ \mathbf{y}_{CR_n} = \boldsymbol{C}_{CR_n}\mathbf{x}_{CR_n} \end{cases} \qquad (14)$$

where

$$\boldsymbol{A}_{CR_n} = \begin{bmatrix} 0 & 1 \\ -\omega_n^2 & -2\omega_n\zeta \end{bmatrix}, \boldsymbol{B}_{CR_n} = \begin{bmatrix} 0 \\ 1 \end{bmatrix} e \qquad (15)$$
$$\mathbf{C}_{CR_n} = \begin{bmatrix} K_{p(v,i)} & K_{Rn(v,i)} \end{bmatrix}$$

$\mathbf{x}_{CRn} = \left[\mathbf{x}^{\alpha}_{CRn}\mathbf{x}^{\beta}_{CRn}\right]^T$ is the controller state, and e is the tracking error.

4. Control based on active damping method

As an alternative to deal with the resonance problem and at the same time guarantee the tracking of the reference sinusoidal signals without including additional losses, active damping method is used in this paper. These consist of the feedback of additional variables (distinct from the controlled variable) to modify the dynamics of the system. One way of carrying out this method is through the multiple loop control strategy [44] where the additional variable is fed back into an internal control loop and the output variable is fed back into the outer loop. In [54] a proposal is introduced to control a three-phase VSI + LCL system connected to the grid based on an equivalent model per phase and two control loops. An external voltage loop on the capacitor and an internal current loop on the capacitor. They are considered only proportional controllers for the two loops.

However, a procedure for determining controller earnings is not described and the choice of feedback variables is not analyzed. The two control loops strategy is also used in [12] to control a three-phase VSI + LCL system connected to the grid. Here the inner loop controls the current, however, for the outer loop the output current is considered. The internal mesh uses a proportional controller, designed to attenuate the resonant behavior and ensure stability. In the external loop, a PR controller is used to track the reference signals with minimal error. The block diagram is shown in figure 3.

Still in [12], the need for the designed controller to guarantee stability in the face of variations in operating conditions (output current and grid inductance values) is highlighted, as well as the tracking of reference signals in the event of external disturbances (mains voltage disturbances). Thus, it is proposed to design a robust control system. The concept of Harmonic Impedance is also introduced, defined as a function of transferring a harmonic disturbance in the mains voltage to the resulting harmonic component in the injected current [55]. With this concept, analytical expressions are presented to measure the sensitivity of the projected controller against disturbances in the mains voltage. However, a criterion for determining the controllers' earnings is not presented, but only an assessment of the effect they have on the stability of the

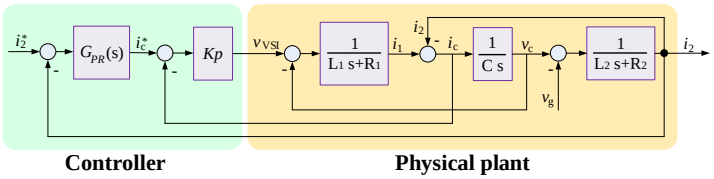

Figure 3: Control scheme (per phase)

system. An analysis of the various control strategies for multiple loops is presented in [44]. The use of several variables in the internal mesh is evaluated considering the rejection of disturbances and the tracking of the reference signal [56]. In this work, the authors were not limited to the case of VSI + LCL systems, but considered the VSI + LC topologies and the case of the current source type inverter with LC output filter. This is important considering that the equivalent model of the VSI + LCL system in autonomous operation can be reduced to a voltage-controlled VSI + LC type system. In addition, the effects of including feedforward loops, decay control and harmonic suppression are analyzed. The effect of the feedback of the additional variable on the internal loop can be analyzed using the transfer functions and the respective Bode diagrams. Initially, consider the transfer functions Gv_{IS} and Gi_{GC} of the inverter output voltage (before the filter) for, respectively, the capacitor voltage in autonomous operation (16), and the output current in connected operation (17).

$$Gv_{IS}(s) = \frac{1}{L_1 C s^2 + R_1 C s + 1} \tag{16}$$

$$Gi_{GC}(s) = \frac{1}{L_1 L_O C s^3 + (L_O R_1 + L_1 R_2) C s^2 + (R_1 R_2 C + L_1 + L_O) s + R_1 + R_2} \tag{17}$$

Capacitor current feedback is considered by means of the proportional gain K_p. Therefore, the transfer functions of the modified Gvc_{IS} and Gic_{GC} plants are defined in (18) and (19).

$$Gvc_{IS}(s) = \frac{K_p}{L_1 C s^2 + (R_1 + K) C s + 1} \tag{18}$$

$$Gic_{GC}(s) = \frac{K_p}{L_1 L_o C s^3 + (L_o R_1 + L_1 R_2 + L_o K) C s^2 + (R_1 R_2 C + L_1 + L_0 + R_2 C K) s + R_1 + R_2} \tag{19}$$

It is observed that the transfer functions obtained are similar to those corresponding to the use of the series resistance method with the capacitor filter. In this case, the term K_p directly modifies the damping factor of the system. To analyze this effect, the respective Bode diagrams are shown in figure 4. The system parameters are listed in Table 1 and K_p is considered equal to the R_d value (passive damping). The diagrams corresponding to the original system according to (16) and (17) are highlighted in blue and those obtained after the current feedback according to (18) and (19) in green. Thus, the damping effect is verified even without the loss of the filtering capacities, resulting in plants that are easier to control through the feedback of the output variable in the external loop. A work similar to that of [44], but considering PI controllers in the external loop, is presented in [57].

However, in this paper the analysis of the effect of the feedback of the variables in the internal loop is carried out in discrete time. Thus, it is concluded that compensators that imply the use of derivatives of variables compromise

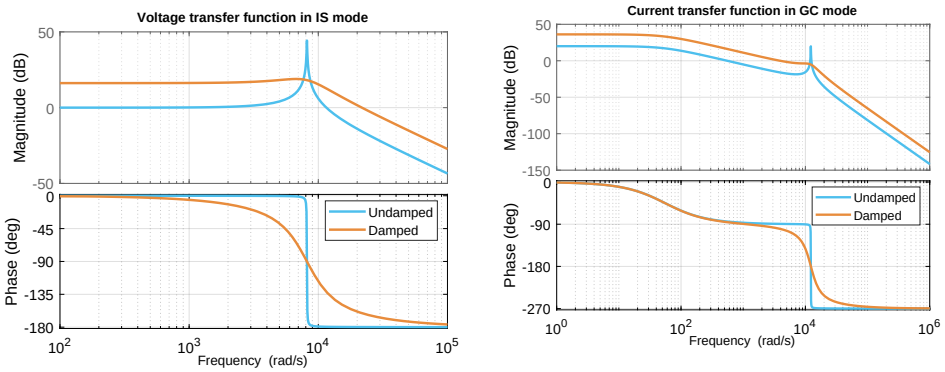

(a) Voltage transfer function in IS mode

(b) Current transfer function in GC mode

Figure 4: Frequency response of the undamped and damped system

the stability of the system at high frequencies. It is observed that the current feedback method in the internal loop has an effect similar to the inclusion of a series resistor with the filter capacitor, for this reason it is known as the virtual resistance method and was initially introduced in [11]. The generalization of this proposal leads to the concept of virtual impedance used in [58] for current source type inverters, and in [59] [60]) where virtual impedances are allocated as the grid interface for avoid coupling between inverters that operate in parallel, a common situation in applications such as UPSs and micro grids. Thus, virtual impedances can be included by means of additional control loops with the purpose of attenuating the resonance of the LCL filter or providing coupling between inverters. A general procedure for designing a multiple loops control system is presented in [59]. This work also introduces a classification for the virtual impedance loops according to their purpose. Internal virtual impedance, that introduced to attenuate resonance; and external virtual impedance, designed for grid connection purposes such as harmonic suppression or interaction with other inverters. The LCL filter is characterized by having a third order behavior. Therefore, to fully describe its dynamics, three state variables are needed, in the case of autonomous operation, two.

However, multiple loop control methods aim to control the system without requiring the sensing of all state variables. The mentioned methods use the feedback (sensing) of two variables (per phase) and transfer functions to deduce the total information of the system dynamics [61], alternatively it is possible to make changes in the filter to obtain variables that allow describe the system with a lower order model, as presented in [62]. Although these methods have an acceptable performance, present high complexity when tuning the different control loops, which can compromise the stability of the system [63]. The sensing of three variables (per phase), which fully describe the dynamics of the system, would facilitate the design of the controllers, but under the criterion of multiple loops, the difficulty of tuning would remain. Furthermore, the control strategy in multiple loops imposes restrictions on the crossing frequency of each loop. Thus, the internal loop must have a crossing frequency higher than the external loop, typically between 5 and 10 times [59]. This, in the case of digital control systems, may imply reduced crossing frequencies in the external loop, limiting the dynamic response of the controlled variable. These limitations lead to considering state feedback control as an alternative. In accordance with [44], to ensure the best performance of the system in autonomous operation, the capacitor current needs to be fed back into the internal control loop, whereas in the operation connected to the grid, it is recommended to feedback the

capacitor voltage. Alternatively, acceptable results are obtained by feedback of the current i_1 in the isolated case, and of the capacitor current in the grid-connected mode. Therefore, there is a need to measure three filter variables to ensure control in both operating modes using active damping techniques. In the case of autonomous operation, the state vector includes the current i_1, thus facilitating the stabilization of the system. In the case of the operation connected to the grid, the capacitor current can be obtained through a simple linear combination of the currents i_1 and i_2 included in the state vector. Therefore, it is possible to perform the active damping of the VSI + LCL system using a state feedback controller according to (20), where u is the control signal, x is the state vector, and K is the feedback gain.

$$\mathrm{u} = K\mathrm{x} \tag{20}$$

The advantage of this strategy is the possibility of synthesizing the proportional gain using several criteria and analytical procedures available in the literature. However, the feedback of the states only guarantees the attenuation of the resonance and, consequently, the stabilization of the system, but not the tracking of reference sine signals. An alternative is the use of additional external grids as in [64], where the system is digitally controlled, considered as state feedback and dead-beat control of the output current. A similar case is presented in [65] where partial state feedback is used to attenuate resonance, and an additional resonant control loop is used to track sinusoidal references and harmonic suppression. In this case, the gains, both in the state feedback and in the resonant control components, are obtained through linear matrix inequalities (LMIs). It should be noted that in both works mentioned, the system is represented in discrete time, considering the delays and the effects of sampling on the controllers' synthesis. However, when considering two control loops, the tuning problem appears every time these loops are designed separately and in some cases, the dynamics of one can influence the stability of the other making tuning an iterative process. This limitation is overcome when the dynamic behavior of the external control loops is represented in state space and included in an enlarged representation of the plant. Thus, the design of the multi-loops tuning can be represented as a single state feedback problem. This criterion is used in [66] to synthesize a state feedback controller for a single-phase VSI + LCL system that operates connected to the grid. In this case, resonant components are included in the fundamental frequency and for the first three odd harmonics. An important point of this work is that the synthesis of the controller is performed in a single procedure using LMIs taking into account the uncertainty in the value of the grid inductance. The representation of control problems through linear matrix inequalities brings important advantages when synthesizing the controller. On the one hand, problems represented as LMIs can be solved using computational procedures [67], which is very useful in high-order systems. For example, in the case presented in [66] after the inclusion of the states of the resonant control, the system is of order twelve. On the other hand, the representation of the control problem through LMIs allows to consider several performance objectives simultaneously for the synthesis of a single controller [68].

5. Robust control based on LMI criterion

The synthesis of controllers using LMIs has important advantages. Among the fundamental ones, we highlight the possibility of synthesizing controllers that simultaneously meet several control objectives, even in the face of variations in some parameters of the system. Applications of LMIs in continuous time for the synthesis of controllers of CC-CC converters are presented in [69]. A similar approach is applied to the single-phase VSI + LCL system in [8], synthesizing robust controllers in a two-loop logic making the islanded and networked operation possible. However, the obtained controllers present a very fast and difficult dynamics in digital systems. Also through continuous time LMIs, [70] proposes a system to control the power injected into the grid by a three-phase VSI + LCL. However, discrete time approaches applied to VSI + LCL systems are presented [65] [66]. The following are presented equations corresponding to the representation using LMIs of the problem of synthesis of controllers by state feedback. In order to take into account the effect of uncertainties, these are considered to be polytopic. This means that the respective expressions of the state-space representation are similar functions of the uncertain parameter [71]. In this way the extreme values of the uncertainty intervals define vertices of a polytope. In each of these vertices the system has a certain dynamics. In this case, if all vertices of the polytope meet the respective inequalities, the LMIs are valid throughout the uncertainty interval [71] [72].

In this section the controller is synthesizing based on the principle of the internal model and using the augmented discrete time state space given as follow:

$$\begin{bmatrix} \mathbf{x}_v \\ d_{syn} \\ \mathbf{x}_{CRnv} \end{bmatrix}_{(k+1)} = \overbrace{\begin{bmatrix} \mathbf{A}_v^k & \mathbf{B}_v^k & \mathbf{0}_{2\times 2h} \\ \mathbf{0}_{1\times 2} & 0 & \mathbf{0}_{1\times 2h} \\ -\mathbf{B}_{CRnv}^k \mathbf{C}_v^k & \mathbf{0}_{2h\times 1} & \mathbf{A}_{CRnv2h\times 2h}^k \end{bmatrix}}^{\mathcal{A}_\mathbf{v}} \begin{bmatrix} \mathbf{x}_v \\ d_{syn} \\ \mathbf{x}_{CRnv} \end{bmatrix}_{(k)} + \overbrace{\begin{bmatrix} \mathbf{0}_{2\times 1} \\ 1 \\ \mathbf{0}_{2h\times 1} \end{bmatrix}}^{\mathcal{B}_\mathbf{v}} u_v + \overbrace{\begin{bmatrix} \mathbf{H}_v^k \\ 0 \\ \mathbf{0}_{2h\times 1} \end{bmatrix}}^{\mathcal{H}_\mathbf{v}} i_2 + \begin{bmatrix} \mathbf{0}_{2\times 1} \\ 0 \\ \mathbf{H}_{CRnv}^k \end{bmatrix} v_{syn} \tag{21}$$

$$z_{v(k)} = \overbrace{\begin{bmatrix} \mathbf{C}_v^k & 0 & \mathbf{0}_{1\times 2h} \end{bmatrix}}^{C_\mathbf{v}} \begin{bmatrix} \mathbf{x}_v \\ d_{syn} \\ \mathbf{x}_{CRnv} \end{bmatrix}_{(k)}$$

$$\begin{bmatrix} \mathbf{x}_i \\ d \\ \mathbf{x}_{CRni} \end{bmatrix}_{(k+1)} = \overbrace{\begin{bmatrix} \mathbf{A}_i^k & \mathbf{B}_i^k & \mathbf{0}_{3\times 2h} \\ \mathbf{0}_{1\times 3} & 0 & \mathbf{0}_{1\times 2h} \\ -\mathbf{B}_{CRni}^k \mathbf{C}_i^k & \mathbf{0}_{2h\times 1} & \mathbf{A}_{CRni2h\times 2h}^k \end{bmatrix}}^{\mathcal{A}_\mathbf{i}} \begin{bmatrix} \mathbf{x}_v \\ d \\ \mathbf{x}_{CRni} \end{bmatrix}_{(k)} + \overbrace{\begin{bmatrix} \mathbf{0}_{3\times 1} \\ 1 \\ \mathbf{0}_{2h\times 1} \end{bmatrix}}^{\mathcal{B}_\mathbf{i}} u_i + \overbrace{\begin{bmatrix} \mathbf{H}_i^k \\ 0 \\ \mathbf{0}_{2h\times 1} \end{bmatrix}}^{\mathcal{H}_\mathbf{i}} v_g + \begin{bmatrix} \mathbf{0}_{3\times 1} \\ 0 \\ \mathbf{H}_{CRni}^k \end{bmatrix} i_{ref} \tag{22}$$

$$z_{i(k)} = \overbrace{\begin{bmatrix} \mathbf{C}_i^k & 0 & \mathbf{0}_{1\times 2h} \end{bmatrix}}^{C_\mathbf{i}} \begin{bmatrix} \mathbf{x}_v \\ d \\ \mathbf{x}_{CRni} \end{bmatrix}_{(k)}$$

The first control objective is to guarantee the stability of the system even in the face of variations in parameters. This leads to the concept of robust stability [73] which can be represented as an LMI, based on Lyapunov's stability criterion, using theorem 1.

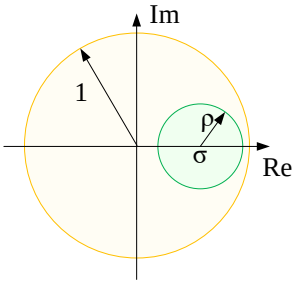

Figure 5: Region $\mathcal{D}$ in the complex plane

Theorem 1. *The uncertain system defined in (21) and (22) are stable within the uncertainty interval if there are symmetric matrices $\mathcal{P}$, and matrices $\mathcal{Q}$ and $\mathcal{L}$ that meet (23).*

$$\begin{bmatrix} \mathcal{P} & \mathcal{A}_{(\mathbf{v},\mathbf{i})}\mathcal{Q} + \mathcal{B}_{(\mathbf{v},\mathbf{i})}\mathcal{L} \\ * & \mathcal{Q} + \mathcal{Q}' - \mathcal{P} \end{bmatrix} > 0 \tag{23}$$

With $\Xi = \mathcal{A}_{(\mathbf{v},\mathbf{i})}\mathcal{Q} + \mathcal{B}_{(\mathbf{v},\mathbf{i})}\mathcal{L}$ and $\Psi = \mathcal{Q} + \mathcal{Q}' - \mathcal{P}$.

If (23) is feasible, the law of robust state feedback control, as defined in (20), is given by (24).

$$\mathbf{K} = \mathcal{L}\mathcal{Q}^{-1} \tag{24}$$

The concept of discrete time stability leads to the allocation of the closed-loop system poles in the circumference of unit radius in the complex plane. This means that the poles can present frequencies up to half the sampling frequency [74]. This situation can lead to problems considering the approach criterion using the average model in a switching period. Therefore, it is considered the possibility to modify the LMI (23) in order to guarantee the robust stability of the system and restrict the closed-loop poles to a specific region of the complex plane. This is done using the discrete time $\mathcal{D}$-Stability criterion [75]. For this purpose, region $\mathcal{D}$ defined in (25) is considered. This region corresponds to the disk with radius ρ and center at σ in the complex plane shown in figure 5.

$$\begin{aligned} &\mathcal{D} = \{z \in \mathbf{C} / \mid z - \sigma \| < \rho\} \\ &\rho, \sigma \in \Re \\ &0 < \rho < 1 \\ &|\sigma| + \rho \leq 1 \end{aligned} \tag{25}$$

Therefore, to synthesize a robust controller by state feedback that ensures that the closed loop poles are within region $\mathcal{D}$, theorem 2 is considered.

Theorem 2. *If there are symmetric matrices $\mathcal{P}$, and matrices $\mathcal{Q}$ and $\mathcal{L}$ that meet (26), therefore, there is the control law according to (24) that stabilizes the systems (21) and (22) and restricts the closed-loop poles to the $\mathcal{D}$ region defined in (25).*

$$\begin{bmatrix} \rho\mathcal{Q} + \rho\mathcal{Q}' - \rho\mathcal{P} & * \\ \mathcal{A}_{(\mathbf{v},\mathbf{i})}\mathcal{Q} + \mathcal{B}_{(\mathbf{v},\mathbf{i})}\mathcal{L} - \sigma\mathcal{Q} & \rho\mathcal{P} \end{bmatrix} > 0 \tag{26}$$

The synthesis of controllers by means of LMIs allows to consider performance objectives such as minimizing the effect of disturbances on a given output. This can be done by considering the LMIs to reduce the $H2$ standard. Thus, the designed

controller aims to minimize the *rms* value of the chosen output due to the disturbances. For this purpose, theorem 3 is considered, where the $H2$ standard of the output z as a function of the disturbances w is kept lower than the value μ.

Theorem 3. *There is a shape controller (24) that guarantees inequality (27), if there exist symmetric positive definite matrices $\mathcal{P}$ and $\mathcal{W}$, matrices $\mathcal{Q}$ and $\mathcal{L}$ such that LMIs (28) are satisfied. [76] [77].*

$$\|\mathbf{H}_{wz}\|_2^2 < \mu \tag{27}$$

$$\begin{aligned} &\text{trace}(\mathcal{W}) < \mu \\ &\begin{bmatrix} \mathcal{W} & C_{(\mathbf{v},\mathbf{i})}\mathcal{Q} + \mathbf{D}_{(v,i)}\mathcal{L} \\ * & \mathcal{Q} + \mathcal{Q}' - \mathcal{P} \end{bmatrix} > 0 \\ &\begin{bmatrix} \rho\mathcal{P} & \mathcal{A}_{(\mathbf{v},\mathbf{i})}\mathcal{Q} + \mathcal{B}_{(\mathbf{v},\mathbf{i})}\mathcal{L} - \sigma\mathcal{Q} & \mathcal{H}_{(\mathbf{v},\mathbf{i})} \\ * & \rho\mathcal{Q} + \rho\mathcal{Q}' - \rho\mathcal{P} & \mathbf{0} \\ * & 0 & \mathbf{I} \end{bmatrix} > 0 \end{aligned} \tag{28}$$

It should be mentioned that, if the uncertainty in the systems is considered, the presented LMIs can be modified by adding sub-index j for matrices $\mathcal{P}, \mathcal{A}_{(v,i)}$ and $\mathcal{B}_{(v,i)}$. Sub-index j indicates that the representation corresponds to a certain vertex of the polytope. Still, the variable $\mathcal{Q}$ is useful only for uncertain systems, so it could be removed from the equation by (29). Thus obtaining LMIs with fewer variables and, consequently, a faster synthesis.

$$\mathcal{Q} = \mathcal{Q}' = \mathcal{P} \tag{29}$$

6. Robust control scheme of DEES

In order to synthesize controllers using LMIs, it is necessary to represent the systems in discrete state space system (21) and (22). For this purpose, equations (4) and (9) are taken at discrete time using the criteria presented in [74]. The parameters involved in this process are shown in Table 1. Generic variables were considered for the representation parameters in discrete time. However, to differentiate the mode of operation, sub-index v is used to designate autonomous operation and sub-index i for operation connected to the grid. A similar procedure is applied to the resonant controller from the state space representation presented in (15). In discrete time, the corresponding controller system matrix is $\boldsymbol{A}_{CRn}^k$, the input matrix is $\boldsymbol{B}_{CRn}^k$, and the state vector is $\mathbf{x}_{CRn}^k$. To obtain a representation of the system that takes into account the effect of the PWM modulator, it is modeled as a unitary delay, similar to that presented in [65] [66]. Therefore, representations (21) and (22) are created for autonomous operation and grid connected, respectively. In these, the state vectors include the physical variables (x_v and x_i), the effect of the unit delay (d_{syn} and d) and the states corresponding to the resonant controllers ($\mathbf{x}_{CRnv}^k$ and $\mathbf{x}_{CRni}^k$). The output variables are, respectively, the voltage on the capacitor for autonomous operation and the current i_2 for operation connected to the grid. For both resonant controllers, components in the fundamental frequency and in the first three additional harmonic components were considered. Considering the state feedback control law (20), the earnings of the controllers are defined. The $\mathbf{K}_v$ gain corresponds to the voltage controller and is obtained from (21). However the $\mathbf{K}_{sys}$ gain, to be obtained based on (22), is the gain corresponding to the joint action of the current and voltage controllers in the grid connected operation. To explain this fact, consider that the gains can be represented according to (30) and (31).

$$\mathbf{K}_v = [\mathbf{K}_{xv} \quad K_{dv} \quad \mathbf{K}_{\xi v}] \tag{30}$$

$$\mathbf{K}_{sys} = [\mathbf{K}_{xsys} \quad K_{i2} \quad K_{dsys} \quad \mathbf{K}_{\xi i}] \tag{31}$$

In this representation, the gains of the control law are separated into components according to the feedback variables. Thus, in the case of the K_v gain, this considers components for the feedback of the state variables (K_{xv}), the control signal (K_{dv}) and the states of the resonant controller ($K_{\xi v}$). The same components are considered in the K_{sys} gain, in this case presented with the *sys* subindex. However, the gain applied to the feedback of the filter variables has been conveniently presented through two components, thus isolating the gain corresponding to current i_2. In this way, the components of the cyclic ratio are generated according to (32) and (33).

$$d_{sync(k+1)} = \begin{bmatrix} \mathbf{K}_{xv} & K_{dv} & \mathbf{K}_{\xi v} \end{bmatrix} \begin{bmatrix} \mathbf{x}_v \\ d_{sync} \\ \xi_v \end{bmatrix}_{(k)} \tag{32}$$

With $\mathbf{K}_{xv} = \left[K_{xv}^{i1},\ K_{xv}^{vc}\right]$, and $\mathbf{K}_{\xi v} = \left[K_{v\xi}^{1},\ K_{v\xi}^{2}\right]$

$$d_{i(k+1)} = \begin{bmatrix} \mathbf{K}_{xsys} & K_{i2} & K_{dsys} & \mathbf{K}_{\xi i} \end{bmatrix} \begin{bmatrix} \mathbf{x}_v \\ i_2 \\ d_i \\ \xi_i \end{bmatrix}_{(k)} \tag{33}$$

With $\mathbf{K}_{xsys} = \left[K_{xv}^{i1},\ K_{xv}^{vc}\right]$, $\mathbf{K}_{\xi i} = \left[K_{i\xi}^{1},\ K_{i\xi}^{2},\ K_{i\xi}^{3},\ K_{i\xi}^{4},\ K_{i\xi}^{5},\ K_{i\xi}^{6}\right]$.

The realization of the feedback gains is made using the control scheme of figure 7. The filter status variables are measured and digitized. Current and voltage tracking errors are applied as input to the current (ξ_i) and voltage (ξ_v) resonant control blocks. Therefore, the control signals are generated from the state variables and the feedback gains according to (32) and (33). As mentioned, the d_i control component is only generated and used in the operation connected to the grid. This is achieved by including a selector on the current controller output and an enabling signal on the resonant control block. In the case of the voltage controller, the resonant controller (ξ_v) is disabled and replaced with a feedforward component by means of the K_{ff} gain.

In the present work, the linear matrix inequalities for synthesis of the controllers were described using the Yalmip® complement on the MatLab® platform, with the chosen solver being LMILab®. Considering the parameters listed in Table 1, as well as the procedure detailed in section 5, the voltage controller gain K_v is:

$$\mathbf{K}_v = [-0.03704\ 8.43e^{-4}\ -0.232\ 201.38\ 3.45\ \ldots 1.81e^{3}\ 3.0211\ 4.798e^{3}\ 1.952\ 6.676e^{3}\ -0.1393] \tag{34}$$

Figure 8 shows the closed-loop Bode diagrams. The tracking of reference signals with a minimum error in the frequency

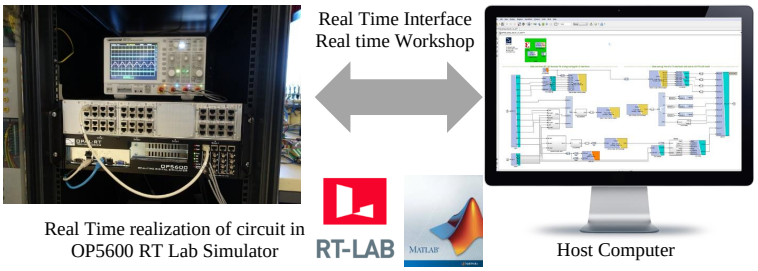

Figure 6: Matlab - OP5600 Real time simulation platforms

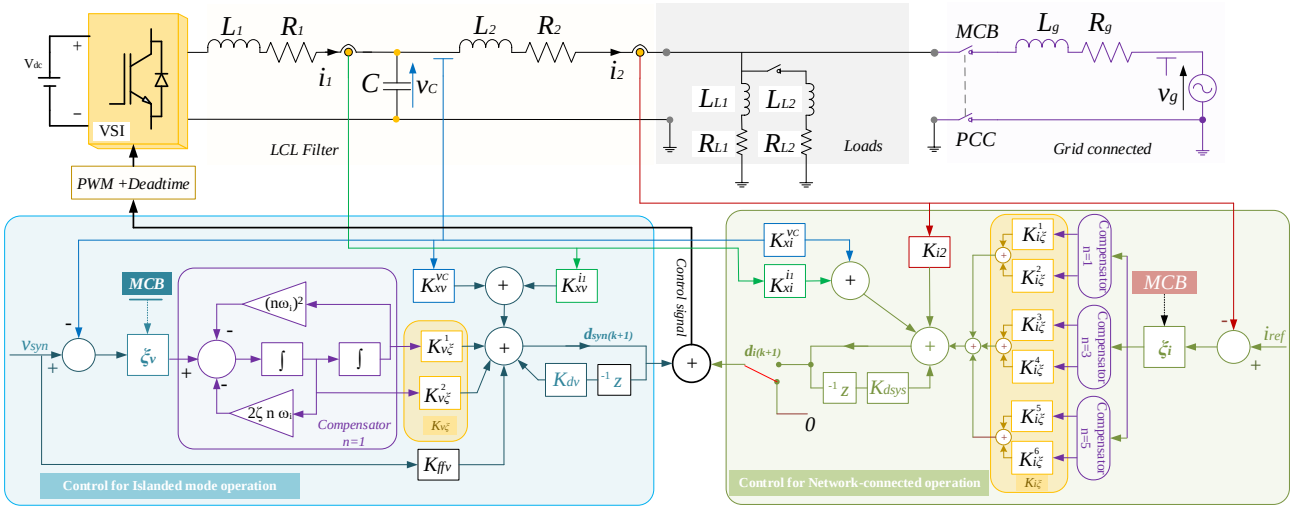

Figure 7: Robust control scheme for single-phase DEES

of $60Hz$ is verified, however the influence of disturbances in the output current is strongly rejected in this frequency and in the first three odd harmonics.

For the determination of the K_{sys} gain, the uncertainty in the grid inductance must be considered within the defined range. This leads to the definition of a two-vertex polytope. In order to reduce the computation time of the solution, the $H2$ minimization LMI is used only for minimum grid inductance conditions. Therefore, the gain obtained was:

$$\mathbf{K}_{sys} = [-0,0637 \;\; -4,394e^{-4} \; 5,022e^{-4} \;\; -0,5256 \;\; -2,505e^{3} \; 21,87 - 1,63e^{4} \; 33,88 \;\; -7,732e^{3} \;\; \ldots \\ 50,50 \; 7,789e^{4} \; 40,15] \tag{35}$$

The controller effect can be seen in the closed-loop Bode diagrams shown in figure 9, which correspond to the extreme values of the uncertainty interval. Figure 9 (a) shows the follow-up of the reference signal, it is observed that the system presents a reduced error for the resonance frequency and the first three odd harmonics. However, in figure 9 (b) it can be seen that the effect of the disturbance on the output current is reduced and still, highly rejected for the resonance frequency, on the considered harmonic components. In this way, it is possible, over the range of possible values for the grid inductance, to trace the reference signal and suppress low-order harmonics due to disturbances in the grid.

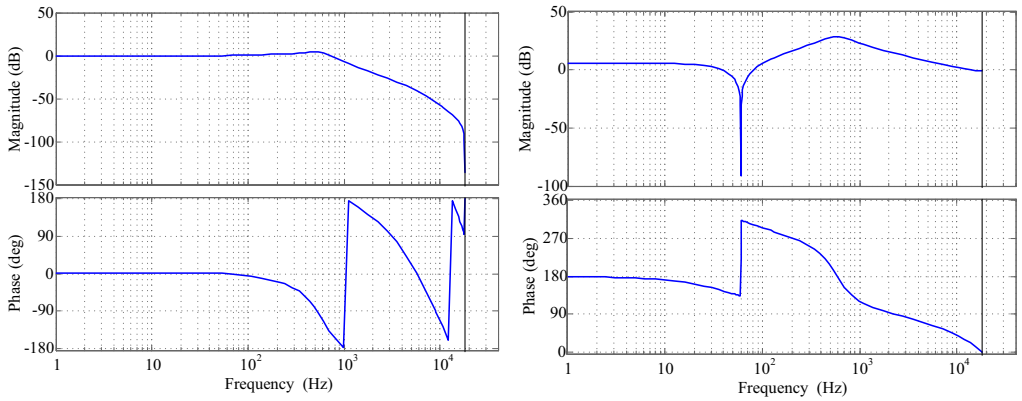

(a) Complementary sensitivity

(b) Sensitivity to disturbances

Figure 8: Closed-loop Bode diagrams in islanded scenario

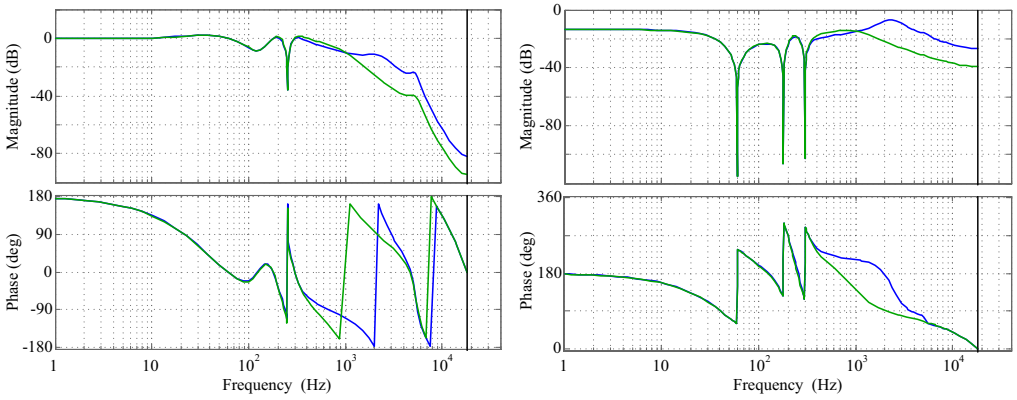

(a) Complementary sensitivity

(b) Sensitivity to disturbances

Figure 9: Closed-loop Bode diagrams in grid connected scenario

Table 1: Parameters for distributed electrical energy systems

System parameters	Variable	Values
Rated power	S_n	$2kVA$
Mains voltage	v_g	$220Vrms$
Grid frequency	f	$60Hz$
Nominal current	i_g	$9.09A$
DC bus voltage	V_{DC}	$480V$
Grid inductance	L_g (range)	$[0:500]\,\mu H$
Grid resistance	R_g	0.01Ω
Deadtime	d_t	$65\mu s$
Switching frequency	f_s	$18kHz$
LCL filters parameters	L_1 R_1	$1mH$ $50m\Omega$
	L_2 R_2	$0.3mH$ $50m\Omega$
	C_1	$3\mu F$
	f_{res}	$3kHz$
Load parameters	L_{L1} R_L	$18mH$ 27.6Ω
	L_{L2} R_{L2}	$18mH$ 27.6Ω

7. Results and discussion

Once the parameters of both control strategies are obtained, they are evaluated by means of computer simulation of the systems. For this purpose, Matlab® Simulink and RT-LAB with OP5600 real time simulator from OPAL-RT platforms was chosen as shown in Figure 6. The first platform is used to describe the control systems, considering their digital realization. The second platform is used for the simulation of the physical systems to be controlled, that is, the VSI + LCL systems (single-phase and three-phase). The control system is made from basic functional blocks available on the platform. Digital components and the effects of sampling and quantization are considered. Still, the dead time effects were included in the power stage model, considering a value of $65\mu s$. The simulations were carried out considering four scenarios corresponding to the two modes of operation and the two transitions between them. The parameters variables and operators described above for the specification of the controller are summarized in Table 1. In order to better visualize the quantities, they are highlighted in color. The capacitor voltage is shown in cyan, the current i_2 in magenta and the mains voltage in blue. To guarantee the transition between operating modes, it is necessary that the control system has a criterion for signal generation and coordination. The criterion used as part of the proposed control strategy is similar to that presented in [78].

7.1. Islanded mode operation

The system is considered to operate initially in autonomous mode. Under these conditions, the control system regulates the voltage on the capacitor to follow the v_{syn} reference signal. The current controller remains disabled. The reference signal is generated internally to meet local load requirements based on previously established information. The voltage controller is designed to reject the effect of disturbances in the load current, this is done through the resonant control components that remain enabled in this operating mode. Therefore, the voltage is regulated against changes in the load

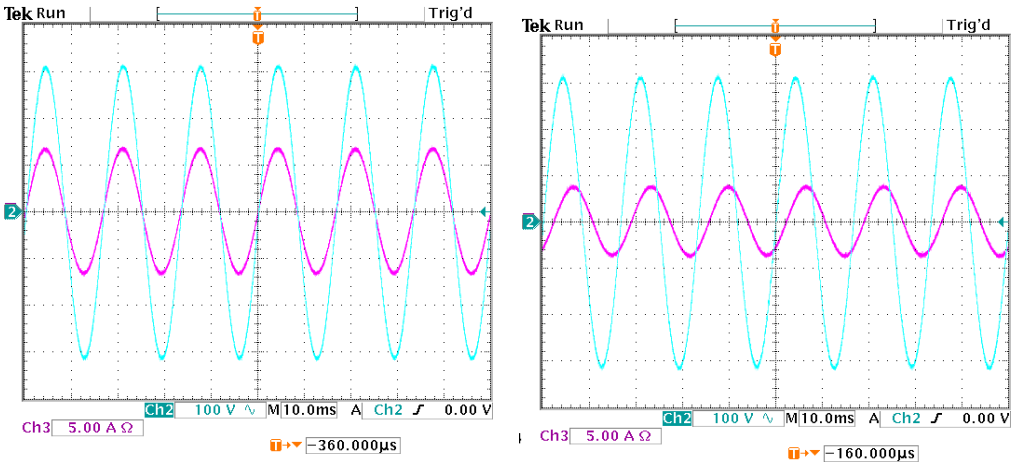

(a) Resistive load

(b) Inductive load

Figure 10: Voltage and current waveforms for island operation

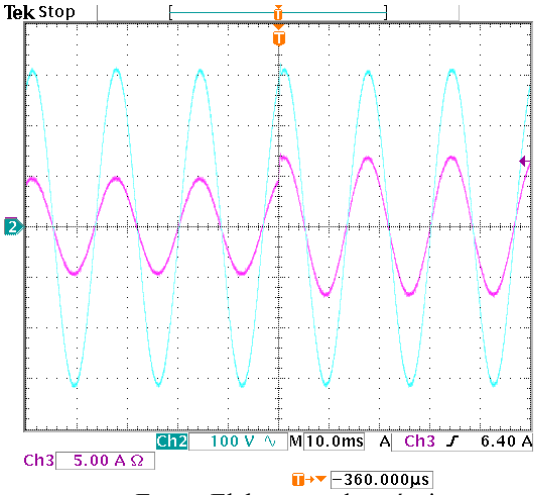

Figure 11: Voltage and current waveforms for island operation with load step

and disturbances in the DC bus voltage. It is verified that in these conditions the only component of the control signal is d_{syn}, generated according to (32) These correspond to the operation with a resistive load $R_{load} = 46\ \Omega$, and with an inductive load $L_{load} = 570$ VA and power factor (PF) $= 0.75$ (inductive). Figs. 10 (a) and (b) show the voltage and current waveforms with a resistive and inductive load for operation in island mode. From this results, we can observe that the proposed control ensures a good responses with fast dynamic and the voltage has the specified amplitude and phase. In the case of operation with resistive load, the voltage presentes a total harmonic distortion (THDv) of only 0.376 %. In the operation with inductive load, the obtained THDv = 0.454 % .

To verify the dynamic response of the proposed controller and the rejection of disturbances in the current, the proposed control system's was evaluated in islanded mode with load step. An initial load of $R_{load} = 770\ W$ and a final load of $R_{load} = 1050\ W$ were considered. The respective voltage and current waveforms are shown in figure 11 From this results, we can observe that, in the step of increasing the load, the voltage practically does not experience sinking with fast dynamic responses and good waveforms of voltage and current in steady state, thus evidencing the fast action of the controller.

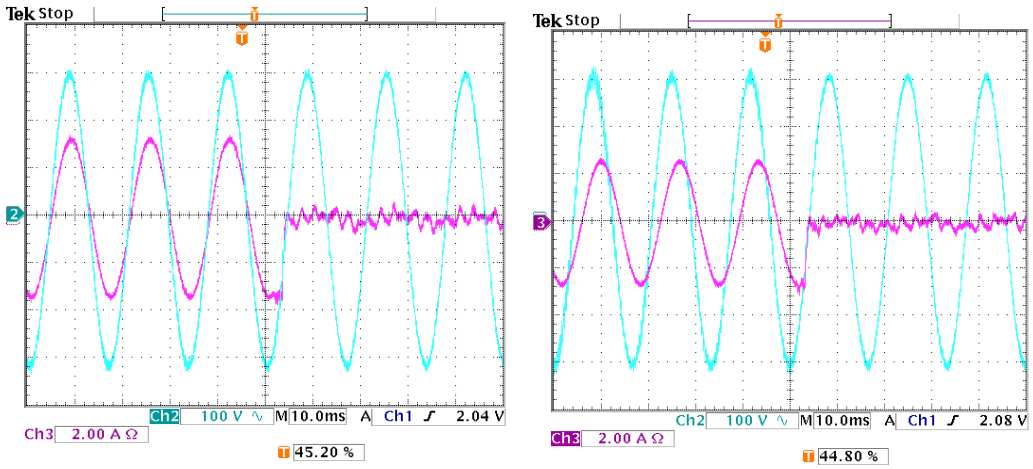

(a) Resistive load

(b) Inductive load

Figure 12: Voltage and current waveforms during the transition to the grid-connected operating mode

7.2. Transition to grid-connected operation mode

Two initial situations were considered corresponding to the islanded operation with a resistive load of $R_{load} = 520\ W$, and with an inductive load of $L_{load} = 440\ VA$ and $PF = 0.8$. Once the grid restoration is confirmed, the voltage reference generation system synchronizes *vsyn* to track the grid voltage. As a consequence, the PCC voltage is reproduced in the LCL filter capacitor. Then, at the peak of the mains voltage, the MCB device is closed and the current controller is reset, but the i_{ref} signal remains null. However, resonant voltage control is disabled. At this point, the effective gain from the joint action of the voltage and current controllers is K_{sys}. The current of i_2 must remain null, otherwise the MCB is opened. The current reference is kept at zero for twelve mains cycles and is then brought to the desired value by means of a ramp. Thus, the system is in operation mode connected to the grid.

The corresponding voltage and current waveforms during connection are shown in figure 12, considering a current scale of 2 A/div. From this results, we can observe a short delay due to the closing time of the MCB device. However, the voltage does not experience considerable transients and the zero current condition is met in both cases. After maintaining the zero current condition for twelve mains cycles, the system operates in the grid connected mode and the current reference is gradually brought using a ramp leading up to the nominal value, corresponding to a power of 2 kW. The voltage and current waveforms (with a scale of 5 A/div), during the ramp in the current reference are shown in figure 13.

7.3. Grid-connected operation

In these conditions, the system must be controlled as a current source, following the sinusoidal reference (i_{ref}) established by the user [12]. Both controllers operate by establishing the K_{sys} state feedback gain. However, resonant voltage controllers are disabled.

The voltage waveforms in the grid and current i_2 for operation connected to the grid with rated power (2 kW) are shown in figure 14. Under these conditions, the injected power in the grid is $R_{load} = 2024.8W$ (with $PF = 0.9972$), a value slightly higher than that requested due to a grid voltage condition higher than the nominal. The current showed a total harmonic distortion of $THD = 1.524\%$.

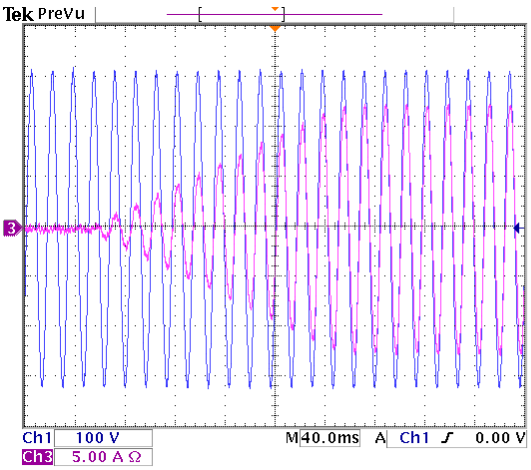

Figure 13: Voltage and current waveforms during the ramp in the current reference

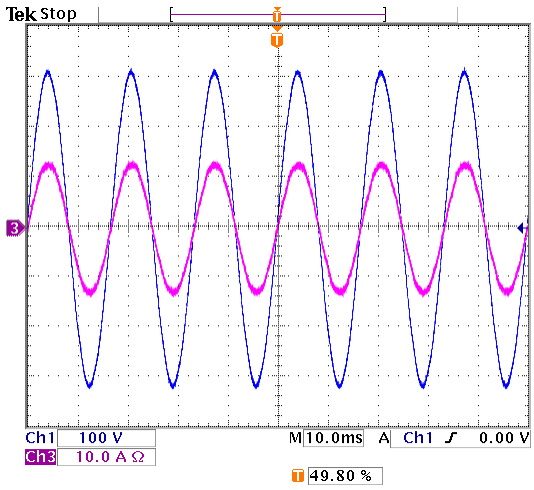

Figure 14: Voltage and current waveforms for operation connected to the grid with rated power (2 kW)

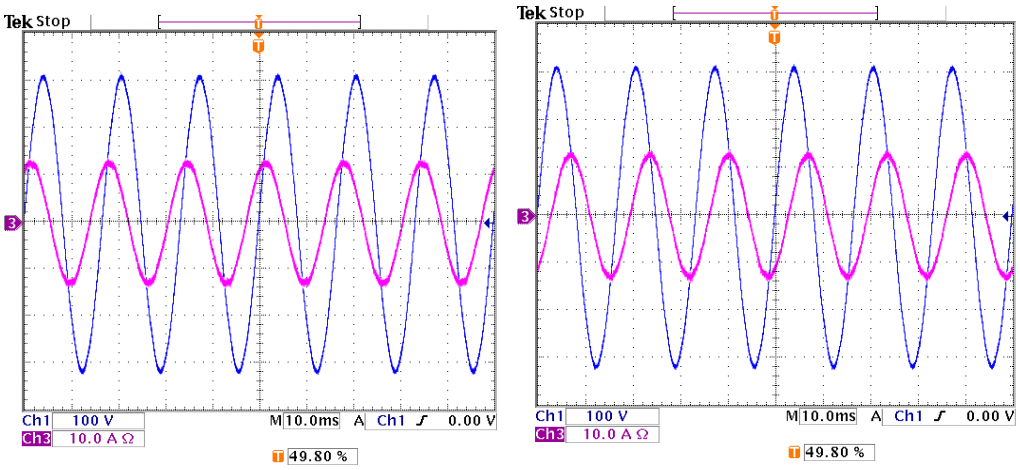

(a) Capacitive current

(b) Inductive current

Figure 15: Voltage and current waveforms for grid-connected operation providing 2 kVA, FP = ± 0.5

In order to analyze the possibility of controlling the injection of active and reactive powers, a reference currents corresponding to 2000 VA with $PF = \pm 0.5$ is used in this test, which corresponds to phase angles of ± 60°. Figure 15 shows the grid voltage and current waveforms for operating conditions connected to the grid with capacitive and inductive references respectively. For the operation providing capacitive current, the apparent power is = 1997.4 VA with $PF = -0.56$ and the harmonic distortion in the current showed THDi = 2.196 %. However, the power dissipated in the damping branch is17.13 W. In the case of operation supplying inductive current, the apparent power = 1998.7 VA is obtained with PF = 0.491 and the harmonic distortion in the current showed THDi = 1.81 % and losses of 20.83 W in the damping industry.

7.4. Transition to islanded mode of operation (islanding)

Due to disturbances in the grid, the system is commanded to switch to the island operation mode. The v_{syn} signal preserves the frequency, initial phase and amplitude values prior to disconnection. The control selector takes the value of d_i to zero, the resonant current controllers are disabled and the current reference signal is brought to zero. However, resonant voltage controllers are enabled. Due to the opening of the MCB, the output current is defined solely by the local load and, therefore, the system is now controlled as a voltage source, thus operating in island mode.

This situation was verified real time considering three scenarios, corresponding to the initial operating condition connected to the grid providing a purely active power reference of 2000 W with unitary, −0.5 and 0.5 power factors. The voltage and current waveforms for each of these scenarios are shown in figures 16 and 17. Similar to the transition to the operation mode connected to the grid, the instant the device opens is delayed. It is observed that the system makes a quick transition to the islanded operation mode, without considerable transients in the capacitor voltage (smooth transition). In the operation connected to the grid, the system is able to control the injected current in compliance with the limits of the IEEE 1547 standard, being able to provide both active and reactive power. In the islanded operation, the system supplies sinusoidal voltage, with reduced THD, to local loads. In both operating modes, the dynamic response is rapid in the event of load variations or the reference signal. Still, the transitions between modes of operation were smooth, without

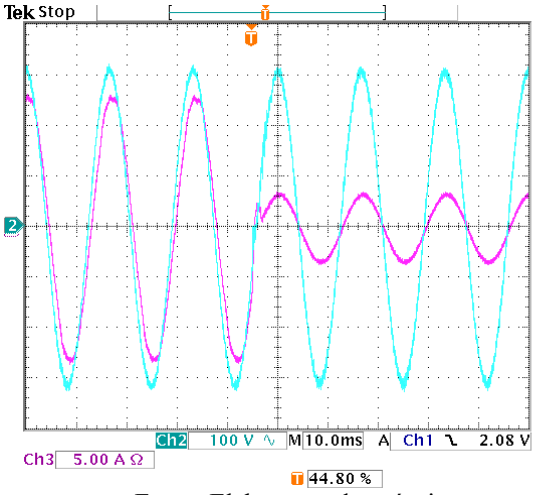

Figure 16: Voltage and current waveforms during islanding, rated power

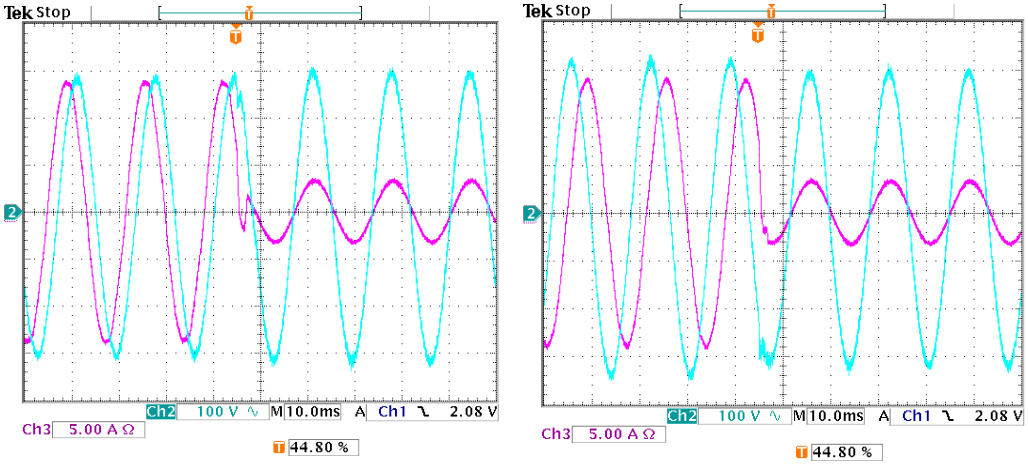

(a) Capacitive current

(b) Inductive current

Figure 17: Voltage and current waveforms during islanding

considerable transients.

8. Conclusion

In this paper, a robust control of voltage source inverter systems with LCL output filter for applications in distributed generation in the microgrid scenario is proposed in both grid and island mode, meeting specific objectives in each mode of operation and with smooth transitions between them. The proposed control of the system was performed by performing the damping using active techniques, considering the criterion of virtual impedance. The system is controlled in both operating modes with a two-loop configuration using proportional resonant-type controllers. The design of the robust controller using LMIs is such that the stability of the system is guaranteed even in the face of variations in the grid inductance with high rejection of disturbances. The real time simulation results obtained validate the design methodology of the damping using active techniques and the proposed control strategy.

References

[1] W. M. Ferreira, I. R. Meneghini, D. I. Brandao, F. G. Guimarães, Preference cone based multi-objective evolutionary algorithm applied to optimal management of distributed energy resources in microgrids, Applied Energy 274 (2020) 115326.

[2] R. Rosso, S. Engelken, M. Liserre, Robust stability investigation of the interactions among grid-forming and grid-following converters, IEEE Journal of Emerging and Selected Topics in Power Electronics 8 (2020) 991–1003. doi:10.1109/JESTPE.2019.2951091.

[3] D. P. e Silva, J. L. F. Salles, J. F. Fardin, M. M. R. Pereira, Management of an island and grid-connected microgrid using hybrid economic model predictive control with weather data, Applied Energy 278 (2020) 115581.

[4] M. F. Zia, E. Elbouchikhi, M. Benbouzid, Microgrids energy management systems: A critical review on methods, solutions, and prospects, Applied Energy 222 (2018) 1033 – 1055.

[5] Q. Wang, W. Yao, J. Fang, X. Ai, J. Wen, X. Yang, H. Xie, X. Huang, Dynamic modeling and small signal stability analysis of distributed photovoltaic grid-connected system with large scale of panel level dc optimizers, Applied Energy 259 (2020) 114132.

[6] S. Chowdhury, Microgrids and Active Distribution Networks, Energy Engineering, Institution of Engineering and Technology, 2009.

[7] F.-s. Kang, S.-J. Park, S. E. Cho, J.-M. Kim, Photovoltaic power interface circuit incorporated with a buck-boost converter and a full-bridge inverter, Applied Energy 82 (2005) 266–283.

[8] C. R. Osório, G. G. Koch, R. C. Oliveira, V. F. Montagner, A practical design procedure for robust h2 controllers applied to grid-connected inverters, Control Engineering Practice 92 (2019) 104157.

[9] A. Akhavan, H. R. Mohammadi, J. C. Vasquez, J. M. Guerrero, Coupling effect analysis and control for grid-connected multi-microgrid clusters, Iet Power Electronics 13 (2020) 1059–1070.

[10] F. Yazdi, S. H. Hosseinian, Variable cost model predictive control strategies for providing high-quality power to ac microgrids, IET Generation, Transmission & Distribution 13 (2019) 3623–3633.

[11] A. Saim, A. Houari, M. Ait-Ahmed, M. Machmoum, J. M. Guerrero, Active resonance damping and harmonics compensation in distributed generation based islanded microgrids, Electric Power Systems Research 191 (2021) 106900.

[12] E. Twining, D. G. Holmes, Grid current regulation of a three-phase voltage source inverter with an lcl input filter, IEEE transactions on power electronics 18 (2003) 888–895.

[13] R. P. Vieira, L. T. Martins, J. R. Massing, M. Stefanello, Sliding mode controller in a multiloop framework for a grid-connected vsi with lcl filter, IEEE Transactions on Industrial Electronics 65 (2018) 4714–4723.

[14] Q. Shi, F. Li, M. Olama, J. Dong, Y. Xue, M. Starke, C. Winstead, T. Kuruganti, Network reconfiguration and distributed energy resource scheduling for improved distribution system resilience, International Journal of Electrical Power & Energy Systems 124 (2021) 106355.

[15] Y. Han, M. Yang, H. Li, P. Yang, L. Xu, E. A. A. Coelho, J. M. Guerrero, Modeling and stability analysis of *lcl*-type grid-connected inverters: A comprehensive overview, IEEE Access 7 (2019) 114975–115001.

[16] M. Shahparasti, M. Mohamadian, A. Yazdian, A. A. Ahmad, M. Amini, Derivation of a stationary-frame single-loop controller for three-phase standalone inverter supplying nonlinear loads, IEEE Transactions on Power Electronics 29 (2014) 5063–5071.

[17] S. Williamson, A. Griffo, B. Stark, J. Booker, A controller for single-phase parallel inverters in a variable-head pico-hydropower off-grid network, Sustainable Energy, Grids and Networks 5 (2016) 114–124.

[18] D. Çelík, M. E. Meral, A flexible control strategy with overcurrent limitation in distributed generation systems, International Journal of Electrical Power & Energy Systems 104 (2019) 456–471.

[19] Y. Tang, W. Yao, P. C. Loh, F. Blaabjerg, Design of lcl filters with lcl resonance frequencies beyond the nyquist frequency for grid-connected converters, IEEE Journal of Emerging and Selected Topics in Power Electronics 4 (2016) 3–14.

[20] M. A. Awal, H. Yu, L. D. Flora, W. Yu, S. Lukic, I. Husain, Observer based admittance shaping for resonance damping in voltage source converters with lcl filter, in: 2019 IEEE Energy Conversion Congress and Exposition (ECCE), 2019, pp. 4455–4462. doi:10.1109/ECCE.2019.8913194.

[21] J. Dannehl, F. W. Fuchs, S. Hansen, P. B. Thøgersen, Investigation of active damping approaches for pi-based current control of grid-connected pulse width modulation converters with lcl filters, IEEE Transactions on Industry Applications 46 (2010) 1509–1517.

[22] Y. Guo, L. Chen, X. Lu, J. Wang, T. Zheng, S. Mei, Region-based stability analysis for active dampers in ac microgrids, IEEE Transactions on Industry Applications 55 (2019) 7671–7682. doi:10.1109/TIA.2019.2913819.

[23] H. Bai, X. Wang, P. C. Loh, F. Blaabjerg, Passivity enhancement of grid-tied converter by series lc-filtered active damper, in: 2015 IEEE Energy Conversion Congress and Exposition (ECCE), 2015, pp. 5830–5837.

[24] Y. Guo, X. Lu, L. Chen, T. Zheng, J. Wang, S. Mei, Functional-rotation-based active dampers in ac microgrids with multiple parallel interface inverters, IEEE Transactions on Industry Applications 54 (2018) 5206–5215. doi:10.1109/TIA.2018.2838058.

[25] S. G. Parker, B. P. McGrath, D. G. Holmes, Regions of active damping control for lcl filters, in: 2012 IEEE Energy Conversion Congress and Exposition (ECCE), 2012, pp. 53–60.

[26] G. Lou, W. Gu, W. Sheng, X. Song, F. Gao, Distributed model predictive secondary voltage control of islanded microgrids with feedback linearization, IEEE Access 6 (2018) 50169–50178.

[27] H. Huerta, A. G. Loukianov, J. M. Cañedo, Passivity sliding mode control of large-scale power systems, IEEE Transactions on Control Systems Technology (2018) 1–9.

[28] Z.-Q. Wu, C.-H. Xu, Y. Yang, Robust iterative learning control of single-phase grid-connected inverter, International Journal of Automation and Computing 11 (2014) 404–411.

[29] H.-K. Kang, C.-H. Yoo, I.-Y. Chung, D.-J. Won, S.-I. Moon, Intelligent coordination method of multiple distributed resources for harmonic current compensation in a microgrid, Journal of Electrical Engineering & Technology 7 (2012) 834–844.

[30] S. Jiang, D. Cao, Y. Li, J. Liu, F. Z. Peng, Low-thd, fast-transient, and cost-effective synchronous-frame repetitive controller for three-phase ups inverters, IEEE Transactions on Power Electronics 27 (2011) 2994–3005.

[31] T. Zhang, M. Huang, X. Chang, Nonlinear backstepping control of grid-connected inverter with lcl high-order filter, International Core Journal of Engineering 7 (2021) 220–229.

[32] M. F. Umar, A. Khan, M. Easley, S. D'Silva, B. Nun, M. B. Shadmand, Resonance suppression based on predictive control of grid-following inverters with lcl filter in weak grid condition, in: 2020 IEEE Energy Conversion Congress and Exposition (ECCE), IEEE, 2020, pp. 4742–4748.

[33] Y. Guan, Y. Wang, Y. Xie, Y. Liang, A. Lin, X. Wang, The dual-current control strategy of grid-connected inverter with lcl filter, IEEE Transactions on Power Electronics 34 (2018) 5940–5952.

[34] X. Zhou, L. Zhou, Y. Chen, Z. Shuai, J. M. Guerrero, A. Luo, W. Wu, L. Yang, Robust grid-current-feedback resonance suppression method for lcl-type grid-connected inverter connected to weak grid, IEEE Journal of Emerging and Selected Topics in Power Electronics 6 (2018) 2126–2137.

[35] L. Jia, X. Ruan, W. Zhao, Z. Lin, X. Wang, An adaptive active damper for improving the stability of grid-connected inverters under weak grid, IEEE Transactions on Power Electronics 33 (2018) 9561–9574.

[36] Z. Ma, L. Zhou, J. Liu, Proportional capacitor current feedback based active damping control for lcl-filter converters with considerable control delay, in: 2020 IEEE Applied Power Electronics Conference and Exposition (APEC), IEEE, 2020, pp. 3110–3114.

[37] M. Malinowski, S. Bernet, A simple voltage sensorless active damping scheme for three-phase pwm converters with an *lcl* filter, IEEE Transactions on Industrial Electronics 55 (2008) 1876–1880.

[38] J. Kukkola, M. Hinkkanen, Observer-based state-space current control for a three-phase grid-connected converter equipped with an lcl filter, IEEE Transactions on Industry Applications 50 (2013) 2700–2709.

[39] J. Dannehl, M. Liserre, F. W. Fuchs, Filter-based active damping of voltage source converters with *lcl* filter, IEEE Transactions on Industrial Electronics 58 (2010) 3623–3633.

[40] X. Tang, W. Chen, M. Zhang, A current decoupling control scheme for lcl-type single-phase grid-connected converter, IEEE Access 8 (2020) 37756–37765.

[41] M. Jian-hui, S. Xin-chun, F. Chao, et al., Optimal control of photovoltaic grid-connected current based on pr control [j], Electric Power Automation Equipment 34 (2014) 42–47.

[42] M. Yuan, Y. Fu, Y. Mi, Z. Li, C. Wang, Hierarchical control of dc microgrid with dynamical load power sharing, Applied Energy 239 (2019) 1 – 11.

[43] V. B. Reddy, N. Harischandrappa, Comparison of phase-shift and modified gating schemes on working of dc-dc lcl-t resonant power converter, IEEE Transactions on Circuits and Systems II: Express Briefs (2020).

[44] S. Wang, L. Lu, X. Han, M. Ouyang, X. Feng, Virtual-battery based droop control and energy storage system size optimization of a dc microgrid for electric vehicle fast charging station, Applied Energy 259 (2020) 114146.

[45] A. M. Bouzid, M. S. Golsorkhi, P. Sicard, A. Chériti, H∞ structured design of a cascaded voltage/current controller for electronically interfaced distributed energy resources, in: 2015 Tenth international conference on ecological vehicles and renewable energies (EVER), IEEE, 2015, pp. 1–6.

[46] R. Teodorescu, F. Blaabjerg, M. Liserre, P. C. Loh, Proportional-resonant controllers and filters for grid-connected voltage-source converters, IEE Proceedings-Electric Power Applications 153 (2006) 750–762.

[47] C. Dong, Q. Gao, Q. Xiao, X. Yu, L. Pekař, H. Jia, Time-delay stability switching boundary determination for dc microgrid clusters with the distributed control framework, Applied Energy 228 (2018) 189 – 204.

[48] T. Toumi, A. Allali, A. Meftouhi, O. Abdelkhalek, A. Benabdelkader, M. Denai, Robust control of series active power filters for power quality enhancement in distribution grids: Simulation and experimental validation, ISA Transactions (2020).

[49] M. Dehghani, A. Kavousi-Fard, T. Niknam, O. Avatefipour, A robust voltage and current controller of parallel inverters in smart island: A novel approach, Energy 214 (2021) 118879.

[50] H. Weng, S. Wang, X. Lin, Z. Li, J. Huang, A novel criterion applicable to transformer differential protection based on waveform sinusoidal similarity identification, International Journal of Electrical Power & Energy Systems 105 (2019) 305 – 314.

[51] M. Eskandari, L. Li, M. H. Moradi, P. Siano, F. Blaabjerg, Optimal voltage regulator for inverter interfaced distributed generation units part: Control system, IEEE Transactions on Sustainable Energy (2020).

[52] X. Yuan, W. Merk, H. Stemmler, J. Allmeling, Stationary-frame generalized integrators for current control of active power filters with zero steady-state error for current harmonics of concern under unbalanced and distorted operating conditions, IEEE transactions on industry applications 38 (2002) 523–532.

[53] C. Liu, X. Li, Y. Zhi, G. Cai, New breed of solid-state transformer mainly combing hybrid cascaded multilevel converter with resonant dc-dc converters, Applied Energy 210 (2018) 724 – 736.

[54] N. Abdel-Rahim, J. E. Quaicoe, Modeling and analysis of a feedback control strategy for three-phase voltage-source utility interface systems, in: Proceedings of 1994 IEEE Industry Applications Society Annual Meeting, volume 2, IEEE, 1994, pp. 895–902.

[55] M. Mahdavyfakhr, N. Rashidirad, M. Hamzeh, K. Sheshyekani, E. Afjei, Stability improvement of dc grids involving a large number of parallel solar power optimizers: An active damping approach, Applied Energy 203 (2017) 364 – 372.

[56] A. E. M. Bouzid, P. Sicard, H. Chaoui, A. Cheriti, Robust three degrees of freedom based on h∞ controller of voltage/current loops for dg unit in micro grids, IET Power Electronics 12 (2019) 1413–1424.

[57] J. Dannehl, F. W. Fuchs, S. Hansen, P. B. Thøgersen, Investigation of active damping approaches for pi-based current control of grid-connected pulse width modulation converters with lcl filters, IEEE Transactions on Industry Applications 46 (2010) 1509–1517.

[58] Y. W. Li, Control and resonance damping of voltage-source and current-source converters with *lc* filters, IEEE Transactions on Industrial Electronics 56 (2008) 1511–1521.

[59] B. Li, W. Yao, L. Hang, L. Tolbert, Robust proportional resonant regulator for grid-connected voltage source inverter (vsi) using direct pole placement design method, IET Power Electronics 5 (2012) 1367–1373.

[60] Y. W. Li, C.-N. Kao, An accurate power control strategy for power-electronics-interfaced distributed generation units operating in a low-voltage multibus microgrid, IEEE Transactions on Power Electronics 24 (2009) 2977–2988.

[61] F. Liu, Y. Zhou, S. Duan, J. Yin, B. Liu, F. Liu, Parameter design of a two-current-loop controller used in a grid-connected inverter system with lcl filter, IEEE Transactions on Industrial Electronics 56 (2009) 4483–4491.

[62] H. Xiao, M. Li, L. Wu, M. Cheng, A novel current controller for grid-connected voltage-source-inverters, IEEE Transactions on Industrial Electronics (2020) 1–1.

[63] M. M. Shabestary, Y. A. I. Mohamed, Asymmetrical ride-through and grid support in converter-interfaced dg units under unbalanced conditions, IEEE Transactions on Industrial Electronics 66 (2019) 1130–1141.

[64] Y. Cai, Y. He, H. Zhou, J. Liu, Active damping disturbance rejection control strategy of lcl grid-connected inverter based on inverter-side current feedback, IEEE Journal of Emerging and Selected Topics in Power Electronics (2020).

[65] J. M. Gonzalez, C. A. Busada, J. Solsona, A robust controller for a grid-tied inverter connected through an lcl filter, IEEE Journal of Emerging and Selected Topics in Industrial Electronics (2020).

[66] L. Maccari Jr, D. Lima, G. Koch, V. Montagner, Robust model predictive controller applied to three-phase grid-connected lcl filters, Journal of Control, Automation and Electrical Systems 31 (2020) 447–460.

[67] P. Ghainet, A. Nemirovski, A. Laub, M. Chilali, Lmi control toolbox-for use with matlab, The Math Works Inc (1995).

[68] S. Boyd, L. El Ghaoui, E. Feron, V. Balakrishnan, Linear matrix inequalities in system and control theory, SIAM, 1994.

[69] P. M. De Almeida, A. Ribeiro, I. Souza, M. Fernandes, G. Fogli, V. Cuk, P. G. Barbosa, P. Ribeiro, Systematic design of a dlqr applied to grid-forming converters, IEEE Journal of Emerging and Selected Topics in Industrial Electronics (2020).

[70] L. P. Sampaio, M. A. De Brito, G. d. A. e Melo, C. A. Canesin, Grid-tie three-phase inverter with active power injection and reactive power compensation, Renewable Energy 85 (2016) 854–864.

[71] A. C. Bartlett, C. V. Hollot, H. Lin, Root locations of an entire polytope of polynomials: It suffices to check the edges, Mathematics of Control, Signals and Systems 1 (1988) 61–71.

[72] J. Ren, F. Li, J. Fu, Robust observer-based finite-time $h\infty$ control for one-sided lipschitz singular systems with uncertainties, IET Control Theory & Applications (2020).

[73] M. C. De Oliveira, J. Bernussou, J. C. Geromel, A new discrete-time robust stability condition, Systems & control letters 37 (1999) 261–265.

[74] K. Ogata, et al., Discrete-time control systems, volume 2, Prentice Hall Englewood Cliffs, NJ, 1995.

[75] K. Furuta, S. Kim, Pole assignment in a specified disk, IEEE Transactions on Automatic control 32 (1987) 423–427.

[76] M. C. De Oliveira, J. C. Geromel, J. Bernussou, Extended h 2 and h norm characterizations and controller parametrizations for discrete-time systems, International Journal of Control 75 (2002) 666–679.

[77] V. F. Montagner, V. J. Leite, P. L. Peres, Discrete-time switched systems: Pole location and structural constrained control, in: 42nd IEEE International Conference on Decision and Control (IEEE Cat. No. 03CH37475), volume 6, IEEE, 2003, pp. 6242–6247.

[78] M. Azab, Multi-objective design approach of passive filters for single-phase distributed energy grid integration systems using particle swarm optimization, Energy Reports 6 (2020) 157–172.